Heliyon 10 (2024) e36731

Contents lists available at ScienceDirect

Heliyon

journal homepage: www.cell.com/heliyon

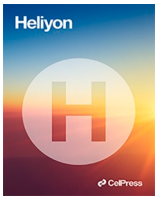

Research article

High removal of methylene blue and methyl violet dyes from aqueous solutions using efficient biomaterial byproduct

Mohammed Alsuhybani [a], Musaad Aleid [a], Reema Alzidan [b], Khaled Bin Bander [a], Ayman Alrehaili [a,*]

[a] King Abdulaziz City for Science and Technology, Riyadh, Saudi Arabia
[b] Princess Nourah bint Abdulrahman University, Riyadh, Saudi Arabia

ARTICLE INFO

Keywords:
Zizyphus spina-christi seeds
Isotherm
Methyl violet
Methylene blue
Mechanism

ABSTRACT

Dyes are among the toxic contaminants that significantly impact water ecosystems. A biomaterial prepared from Zizyphus Spina-Christi seed (ZSCS) to remove methylene blue (MB) and methyl violet (MV) from an aqueous solution was investigated. Several techniques have been used, including FTIR, SEM, EDX, XPS, and TGA, to characterize the physical and chemical properties of ZSCS. The effect of various parameters such as pH, adsorbent dosage, contact time, temperature, and initial dye concentration on the adsorption process were studied. The ZSCS adsorbent showed efficient MB and MV dye adsorption with Langmuir adsorption capacity of 666.66 and 476.19 mg/g, respectively, at experimental condition [(pH = 6; time = 30 min; T = 45 °C, dye concentration: 500 mg/L, and adsorbent dose = 0.6 g/L for MB and 1 g/L for MV dye)]. Kinetic and isotherm models were applied to fit the experimental outcomes. The result showed that ZSCS showed an ultrafast absorption process with a high removal efficiency of MB and MV within 5 min indicating its effective adsorption properties. The Langmuir isotherm model was the most suitable model for describing the adsorption of MB and MV dyes on ZSCS. The pseudo-second-order model kinetic fits better to MB and MV adsorption onto ZSCS than other models, suggesting that the adsorption mechanism followed chemisorption. Our results could offer an efficient cost-effective approach for dye removal from wastewater.

1. Introduction

The global challenge of insufficient drinking water has arisen because of extensive industrialization and urbanization, continually jeopardizing water resources [1]. The water scarcity issue extends beyond the availability of water resources; it is increasingly associated with water quality degradation resulting from toxic pollution and human interventions in the water cycle and natural processes [2–4]. Various industries, such as textiles, cosmetics, and food, released effluents, influencing water environments. With the increasing overall demand for water, there is a continuous rise in worldwide wastewater production, emphasizing the necessity for effective purification methods [5]. Water pollution stemming from dyes has emerged as a significant global concern in recent years, attracting widespread attention [6]. There are more than 100,000 diverse industrial organic dyes and pigments, with overall production reaching several tons annually [7–9]. Therefore, the environmental impact is exacerbated by the spilling of dyes into the water ecosystem during both manufacturing and practical use, posing substantial challenges [10,11]. Dyes are classified into three

* Corresponding author.
E-mail address: amalharbi@kacst.gov.sa (A. Alrehaili).

https://doi.org/10.1016/j.heliyon.2024.e36731
Received 29 March 2024; Received in revised form 17 July 2024; Accepted 21 August 2024
Available online 29 August 2024

categories: cationic, anionic, and nonionic. Among these dyes, cationic dyes are more toxic than anionic dyes [12]. These dyes often contain carcinogenic substances or pose toxic risks to the health of humans and other living organisms [8,13–16]. The global water quality is further compromised, as wastewater contaminated with dyes is deemed harmful to ecosystems, human health, and aquatic environments [17]. Its adverse effects on humans and animals underscore the urgent need for proper attention and management.

Among the cationic dyes, methylene blue (MB) and methyl violet (MV) are extensively utilized and are presently acknowledged as the most prevalent and perilous dyes [18,19]. These dyes are widely utilized in dying and textile industries for coloring [20]. Generally, MB and MV are difficult to biodegrade, highly soluble in water, and carcinogenic, posing a threat to human health and aquatic life [21]. Direct contact with these dyes can cause permanent damage to humans and animals, along with additional severe effects due to its toxicity [22]. High levels of MB and MV can disrupt the metabolism of microalgae and interrupt photosynthesis processes, leading to instability in the aquatic ecosystem [23–25]. In humans, MB and MV are able to cause various health issues such as allergies and cancer [26]. Consequently, there is significant environmental concern regarding treating effluents contaminated with such dyes that are hard to remove from wastewater using conventional methods [27].

However, various technologies, including photocatalytic degradation [28,29], adsorption [30–32], biological treatment [33], detoxification [34], and electrochemical degradation [35] have been employed to cope with dyes in aqueous media. One of the best approaches is to use adsorption, a separation process that involves increasing the number of chemical components at the surface of a solid [36]. It is considered an effective and preferred approach for reducing the concentration of pollutants in wastewater due to its affordability, simple design, efficient pollutant removal, easy operation, and availability. Many materials are employed for the adsorption methods. Among these materials, agricultural byproducts are widely used due to their accessibility, eco-friendly, cost--effectiveness, minimal processing time, and cheaper and abundantly available materials [37–40]. Several agricultural byproducts, such as *Citrus sinensis* leaf [41], potato peel [42], almond shell [43], pine tree leaves [44], garlic peel [45], and walnut shells [46], have been implemented in the adsorption processes.

Ziziphus spina-christi (ZSC) can be a promising choice as an adsorbent due to its availability and affordability [47,48]. ZSC is native to regions in the Middle East, having adapted to arid and semi-arid environments. It is known for its hardiness in challenging conditions; the plant's fruit is also utilized in traditional medicine [47,48]. Numerous studies indicate that the ZSC byproducts can be implemented to remove heavy metals and dyes from aqueous solutions. A group of researchers pointed out that activated carbon prepared using Ziziphus spina-christi seed (ZSCS) successfully removed malachite green dye [49] manganese [47]. Although ZSCS with activated carbon method is widely used, it is still not commonly affordable. Hence, the focus should be shifted toward exploring a cost-effective biomaterials product. Another study showed that the ZSCS could remove cadmium [48] from an aqueous solution without implementing further materials. However, there needs to be more emphasis on removing MB and MV using ZSCS.

In this context, the primary goal of our research is to shed light on an effective method for removing MB and MV from wastewater effluent. We will explore a cost effective elimination of MB and MV in an aqueous solution using ZSCS, a biomaterial byproduct. The adsorption capacity and removal efficiency of the new adsorbent in eliminating MB and MV from aqueous solutions under optimal operating conditions are assessed. The experimental findings will be subjected to thermodynamics, equilibrium, and kinetic processes to elucidate the attributes of the adsorption mechanism.

2. Materials and methods

2.1. Materials

Hydrochloric acid (37 %, Scharlau lab, Spanish), sodium hydroxide (98 %, Polskie Odczynniki Chemiczne (Gliwice, Poland), acetone (99.5 %, Panreac Sintesis, Barcelona, Spain), Ethanol (99.9 %, Scharlau lab, Spanish), methylene blue (Laboratory-stain for microscopy C.l.NO. 52015, India), methyl violet (Loba Chemie, Mumbai, India).

2.2. Sample preparation

A 10 g of the seeds were grinded using a jaw crusher and then washed through a filter (0.45 μm, Dorsan) using 500 ml distilled water to eliminate impurities. The filter was dried at 60 °C for 24 h in an oven, and then the material cumulated on the filter was collected and sifted by successive sieves (JVLAB, 250 μm). First, the standard solution of MB with 1000 ppm concentration was prepared using 1 g of dye placed in a 1 L standard beaker (Schott, Germany). Second, a 50 ppm standard solution was prepared, and then pH was adjusted to 7 using 0.1M hydrochloric acid and 0.1M sodium hydroxide, monitored by a pH device (JENWAY model 3510 pH Meter). Third, 0.05 g of the adsorption substance, ZSCS, was added to 50 ml of the solution prepared in the previous step. Fourth, it was put in a water bath (GFL model 1086) for 24 h at 25C with 200 speed shaking. Fifth, the solution was filtered by a paper filter (0.45 μm, DORSAN), and the concentration of MBD was measured using Ultraviolet and Viable light (UV–VIS) (PerkinElmer model Lambda 365) at 663 nm wavelength.

2.3. Instrument

Fourier transform infrared spectroscopy (FTIR, Nicolet 6700, USA) was used to analyze the functional groups in the 400-4000 cm-1 range using the KBr disc method with 32 scans. Analysis was conducted in the range of 5–100° 2θ. Thermogravimetric analysis (TGA) was performed using a Mettler Toledo GA/SDTA851 instrument to evaluate the thermal stability of ZSCS. TGA analysis was conducted over a 30–1000 °C temperature range with a heating rate of 20 °C/min under a dynamic nitrogen (N_2) atmosphere. X-ray

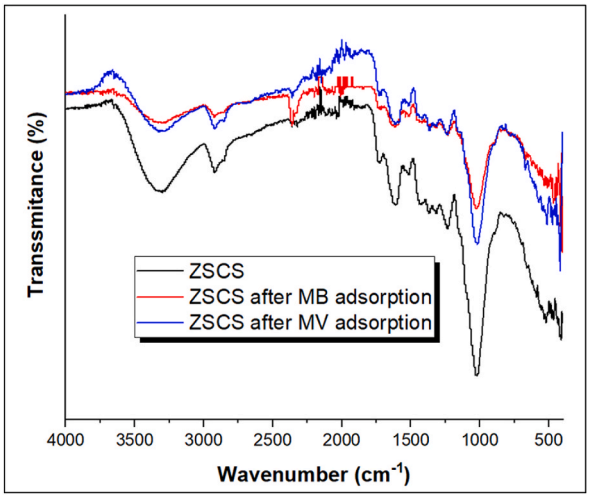

Fig. 1. FTIR spectra of ZSCS adsorbent before and after dyes adsorption.

photoelectron spectroscopy (XPS) analysis was performed using a JPS-9200 XPS spectrometer manufactured by JEOL. Scanning electron microscopy (SEM) was used to magnify the sample surface from 1 to 20 μm using the JSM-7100F instrument by JEOL. The zeta potential of ZSCS was obtained by a Zetasizer Nano ZS instrument (Malvern, UK).

2.4. Batch adsorption experiments of dyes

Batch adsorption experiments were performed in aqueous solutions to evaluate the ability of ZSCS adsorbent to remove MB and MV dyes from aqueous mediums. The influence of various parameters such as amount of the adsorbent (0.4–6 g/L), pH (2–10), contact time (5–120 min), temperature (25–45 °C), and initial MB and MV dye concentrations (50–500 mg/L) were investigated. Generally, 0.4 and 1 g/L of the ZSCS adsorbent were added to the 50 ml of MB (50 mg/L) and MV (50 mg/L) solutions, respectively, (separately and in individual containers). NaOH and HCl were utilized to fix the pH of the solutions at desired value. Thereafter, the samples were placed in a temperature-controlled shaker at 100 rpm for 120 min. Then, the adsorbents were separated from the solutions, and the residual MB and MV dyes were determined by Ultraviolet and Viable light (UV–VIS) (PerkinElmer model Lambda 365) at $\lambda_{max} = 584$ nm for MV dye and $\lambda_{max} = 663$ nm for MB dye. The removal efficiency (%R) and adsorption capacity (mg/g) were determined according to Eqs. (1) and (2), respectively.

$$\%\,R = \frac{Co - Ce}{Co} \times 100 \tag{1}$$

$$qe = (Co - Ce)\frac{V}{m} \tag{2}$$

where C_o (mg/L) and C_e (mg/L) represent the initial and final concentration of dyes, V(L) denotes the volume of solution, and m (g) denotes the amount of ZSCS adsorbent.

3. Results and discussion

3.1. Characterization of adsorbent

FTIR spectra of the ZSCS adsorbent is shown in Fig. 1. The prepared ZSCS powder adsorbent presented characteristics bands at 3307, 2928, 2850, 1729, 1615, 1511, 1431, 1365, 1312, 1233, and 1019 cm^{-1} attributed to tannins, phenols, protein, alkaloids, saponin, glycosides, and flavonoid molecules in ZSCS powder [50,51]. In detail, the broadband at 3307 cm^{-1} is due to the stretching vibration of overlapping –OH with -NH present in the above molecules [52]. The absorption bands at 2928, 2850, 1729, and 1615–1511 cm^{-1} were attributed to stretching vibration of asymmetrical ν(C–H), symmetrical ν(C–H) methyl group, and ν(C=O) in carboxylic acid. The two bands at 1615 and 1511 are attributed to ν(C=C) stretching in aromatic rings [52]. The other bands at 1431, 1365, 1312, 1233, and 1019 cm^{-1} are due to C–H asymmetric deformation, $–CH_2$ scissoring, C-N, C–O, and C-O-C stretching in tannins, protein, Alkaloids, Saponin, Glycosides, Flavonoid, molecules [52]. After the adsorption of MB and MV on the ZSCS adsorbent, it was observed that all the bands decreased in intensity with slight shifts indicating the bending of the dyes on the surface adsorbent. In detail, the intensities of the bands at 3307 and 1729 cm^{-1} for the –OH/-NH and –COOH groups were reduced and shifted to (3312 cm^{-1}, 1725 cm^{-1}) and (3307 cm^{-1}, 1726 cm^{-1}) after the adsorption of MV and MB, respectively. This is due to the electrostatic attraction between the cationic MV and MB molecules and the negative charge of COO- on the ZSCS adsorbent. In addition, the C=C

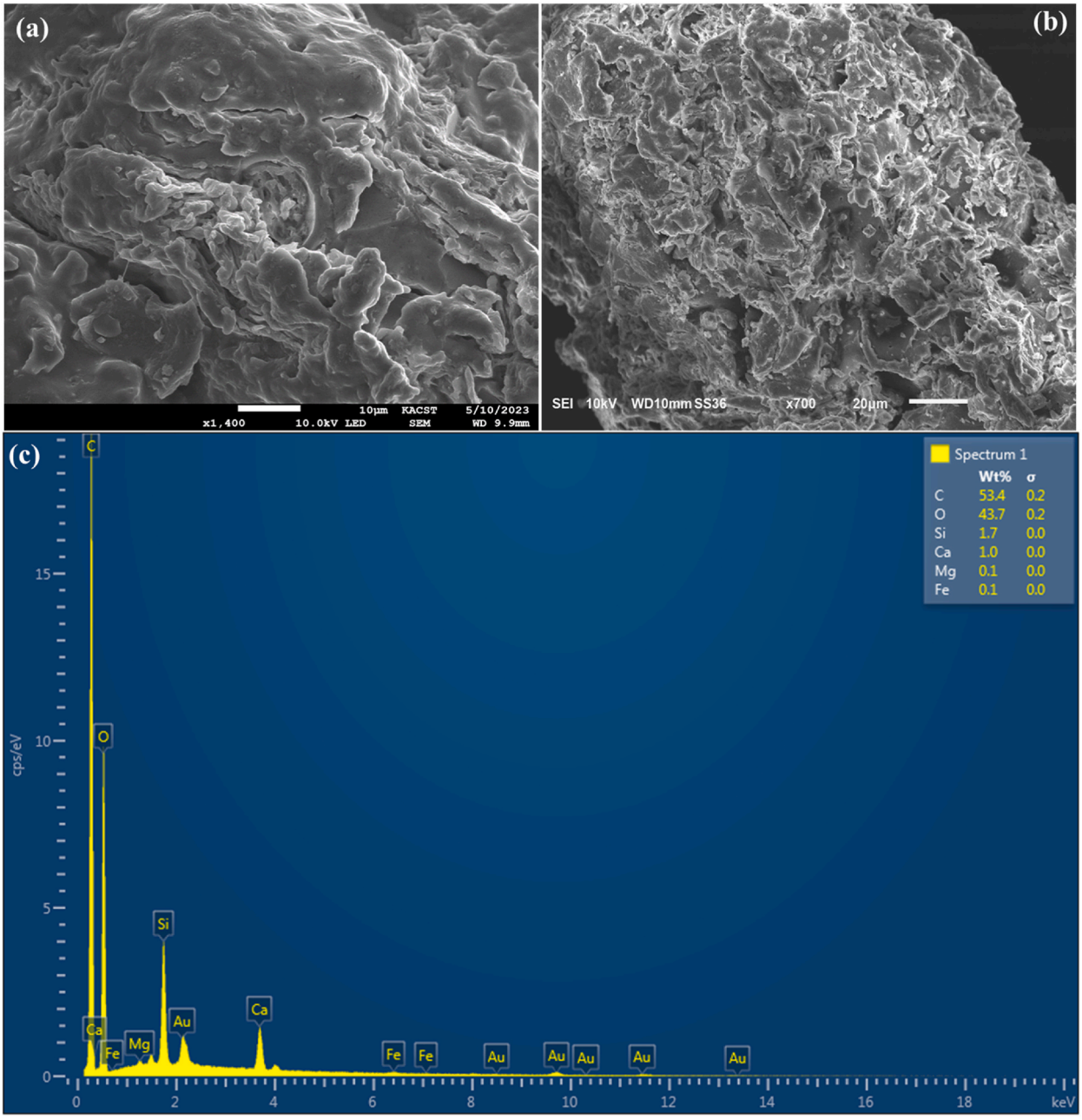

Fig. 2. SEM images of untreated ZSCS (a) treated ZSCS (b), EDX analysis of ZSCS adsorbent.

bond intensity decreased after dyes due to π–π interactions between dye molecules and aromatic rings in the ZSCS sorbent. Overall, the low density of functional groups after adsorbed dyes confirmed the successful adsorption of MV and MB dyes on the ZSCS adsorbent surface via π–π interactions, electrostatic interaction, and hydrogen bonding.

The surface morphology of raw ZSCS and processed ZSCS powder was analyzed by SEM, as shown in Fig. 2. It was observed that the surface of the ZSCS powder showed rough surfaces with many cavities (Fig. 2b), which reflects the higher dye absorption compared to the surface form of raw ZSCS, which showed smooth surfaces (Fig. 2a). The elemental analysis of ZSCS adsorbent was analyzed by EDX analysis, as shown in Fig. 2c. EDX spectrum showed major element compositions for carbon (53.4 %) and oxygen (43.7 %) with traces of elements such as silicone (1.7 %), calcium (1.0 %), magnesium (0.1 %), and iron (0.1 %).

The thermogravimetric analysis (TGA) curve of ZSCS powder is presented in Fig. 3a. The entire heat range was divided into three stages, namely 25–100 °C, 100–450 °C, and 450–1000 °C. The total weight loss was ~90 % at temperatures between 25 °C and 1000 °C. In the first stage, a weight loss of ~5 % was observed in the temperature between 25 and 180 °C due to moisture loss in the

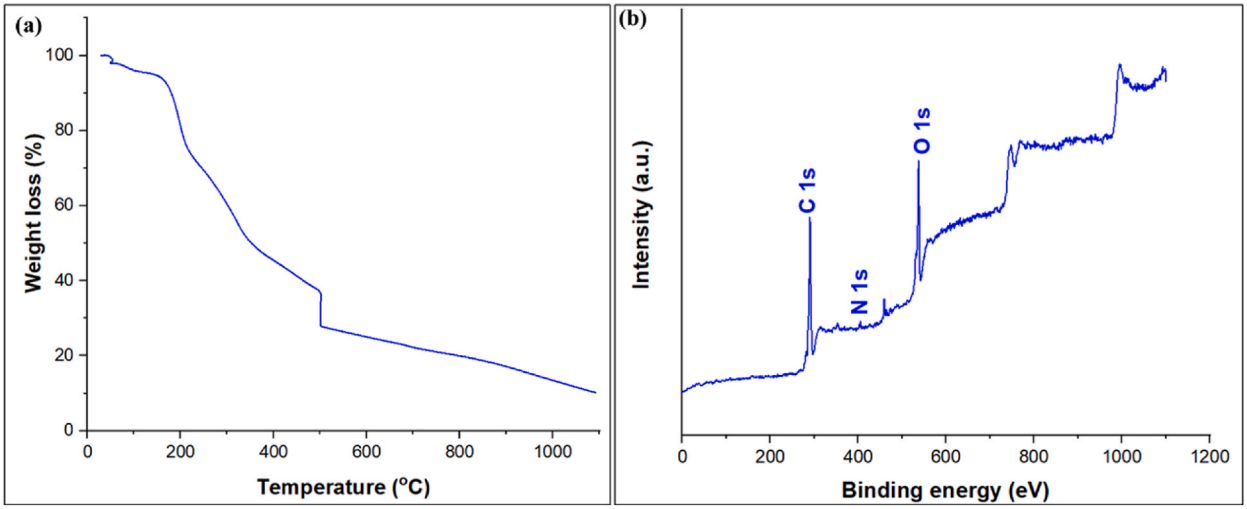

Fig. 3. TGA curve (a) and XPS wide survey spectra of ZSCS adsorbent (b).

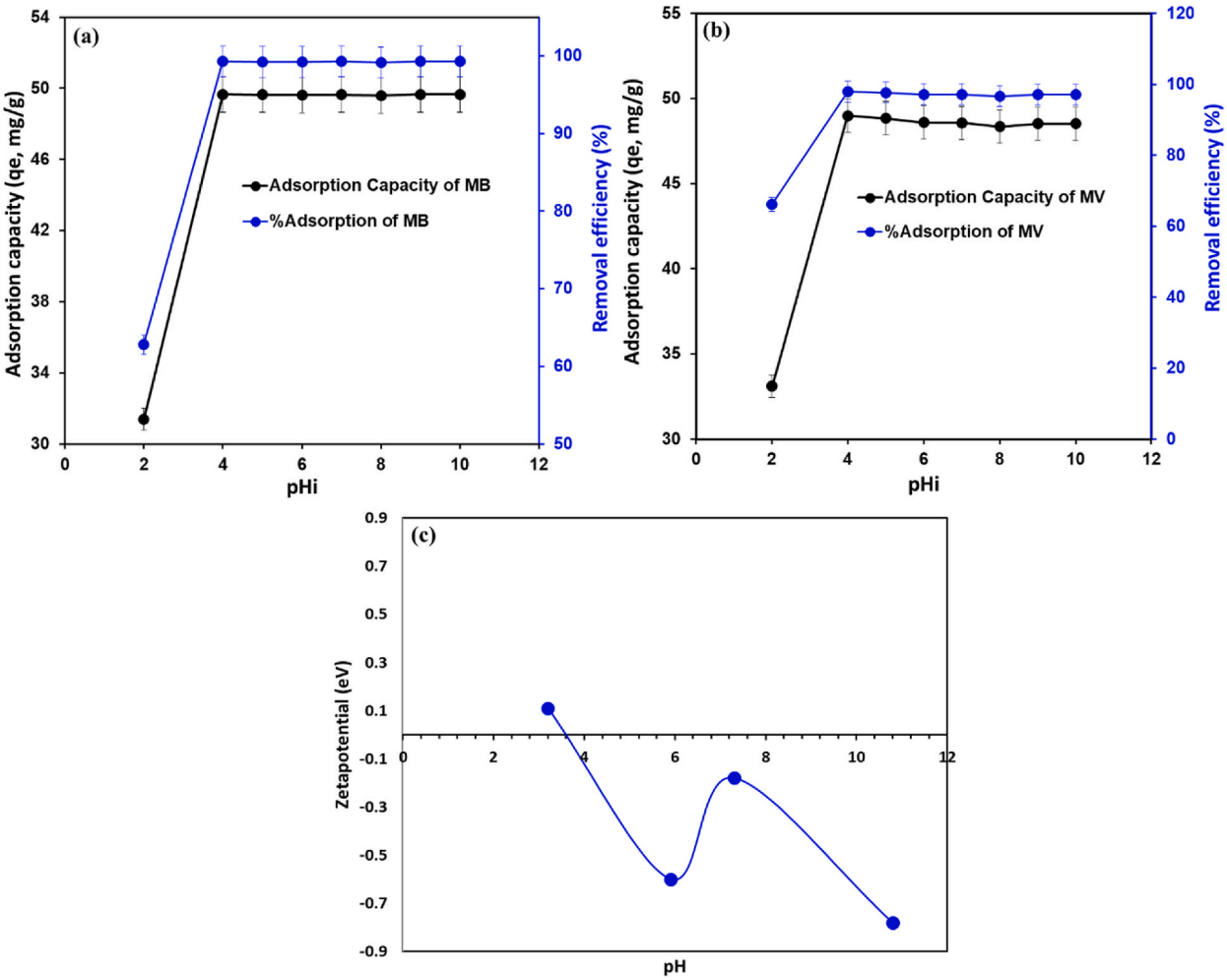

Fig. 4. Influence of pH on the adsorption of MB (a) and MV (b) [(C_o = 50 mg/L; time = 1440 min; T = 25 °C, and adsorbent dose = 1 g/L)]. Zeta potential of ZSCS adsorbent at different pH (c).

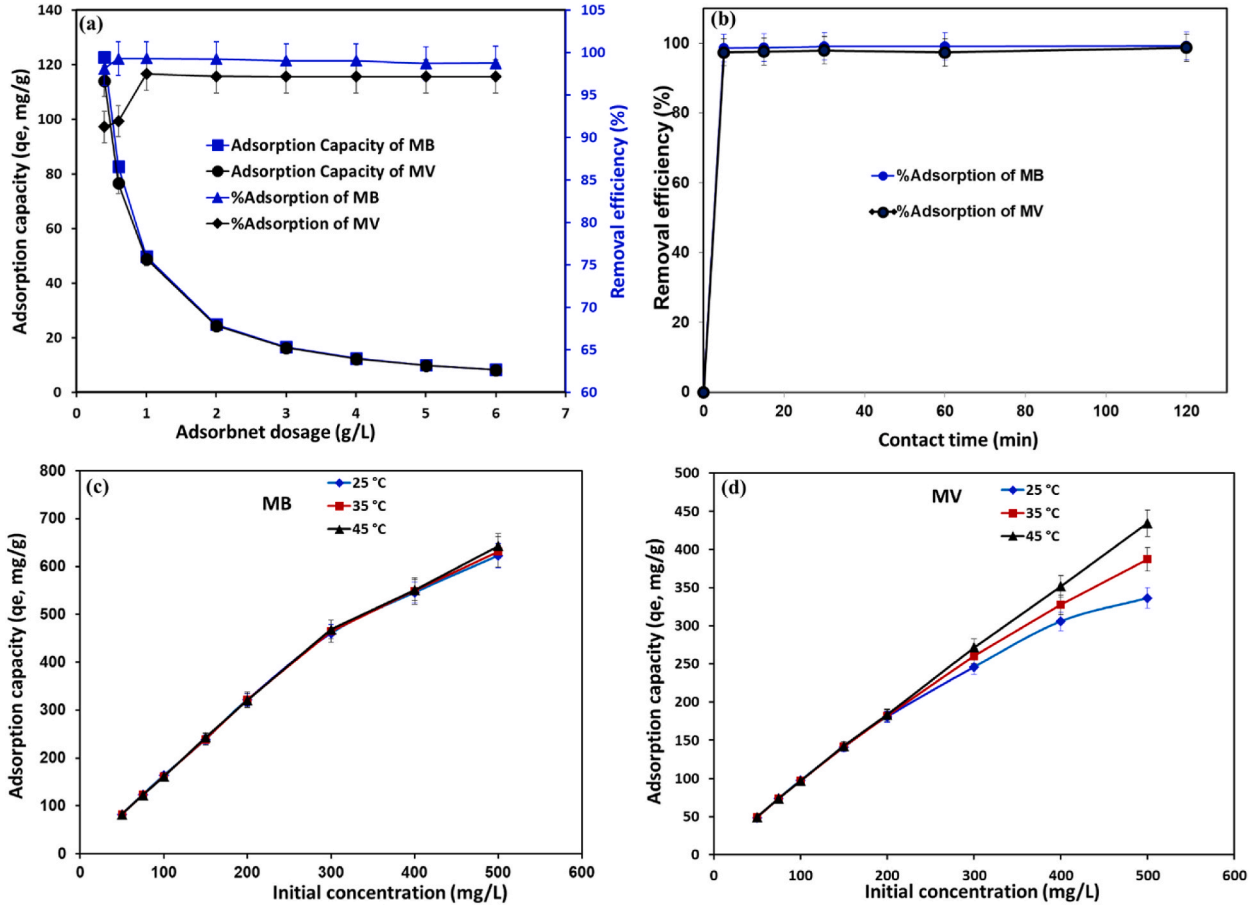

Fig. 5. Influence of adsorbent dosage [(C_o = 50 mg/L; time = 30 min, pH = 6; T = 25 °C)] (a), contact time (b) and initial dye concentration on the adsorption of MB (c) and MV dye(d) on ZSCS adsorbent [(C_o = 50–500 mg/L; time = 30 min; pH = 6; T = 25–45 °C, and adsorbent dose = 0.6 g/L for MB and 1 g/L for MV dye)].

ZSCS powder. The main degradation occurred between the temperatures 100–450 °C with ~67 % weight loss attributed to the decomposition of chemical components of ZSCS sample such as lignin, tannins, phenols, protein, alkaloids, saponin, glycosides, and flavonoid molecules. In the third stage, there is an 18 % weight loss between the temperatures 450–1000 °C due to the degradation of lignin [47]. The surface elemental composition of ZSCS powder was analyzed by X-ray photoelectron spectroscopy, and the results are presented in Fig. 3b. Survey spectra of the sample showed three peaks at 285.3, 400, and 532.4 eV attributed to C 1s, N 1s, and O 1s, respectively.

3.2. Adsorption parameters

3.2.1. Effect of pH

The effect of pH on the adsorption rate of MB and MV dye on the ZSCS adsorbent was tested by varying pH values over the range of 2–10 at constant parameters (C_o = 50 mg/L, time = 1440 min, adsorbent dose = 1 g/L, and T = 25 °C), as shown in Fig. 4a and b. The results revealed that the adsorption rate of MB and MV dyes significantly increased from 66.80 % to 99.30 % for MB and 66.20 %–97.96 % for MV with increasing the pH from 2 to 4 and then became constant with further increases of pH from 4 to 10 increased. The zeta potential of ZSCS material is pH_{Zpc} = 3.8, as shown in Fig. 4c. This indicates that the surface of ZSCS is positively charged at pH_{zpc} < 3.8 and negatively charged at pH_{zpc} > 3.8. When pH_{Zpc} < 3.8, the adsorption capacities of MB and MV were low, due to the competition of the dye with H^+ ions and cationic dyes for the active site above the surface of the adsorbent in an acidic solution, moreover, the increase of adsorption capacity at pH = 3.8 is due to the participation of reaction π–π interactions and H binding in dye absorption. The increase in removal efficiency and adsorption capacity at pH_{Zpc} > 3.8 can be attributed to the adsorption of dyes via electrostatic interaction between the negative charge of the surface adsorbent and the positive charge of the cationic dyes in addition to the two mechanisms mentioned above. The maximum adsorption capacity of ZSCS towards MB and MV efficiency for MB and MV dyes was 49.65 and 48.95 mg/g, at a pH range of 4–10, respectively. There was no significant difference between the removal rate at pH 4 to 10. Therefore, pH 6 was chosen as the optimal pH for future experiments. Similar results have been reported on the influence of pH on

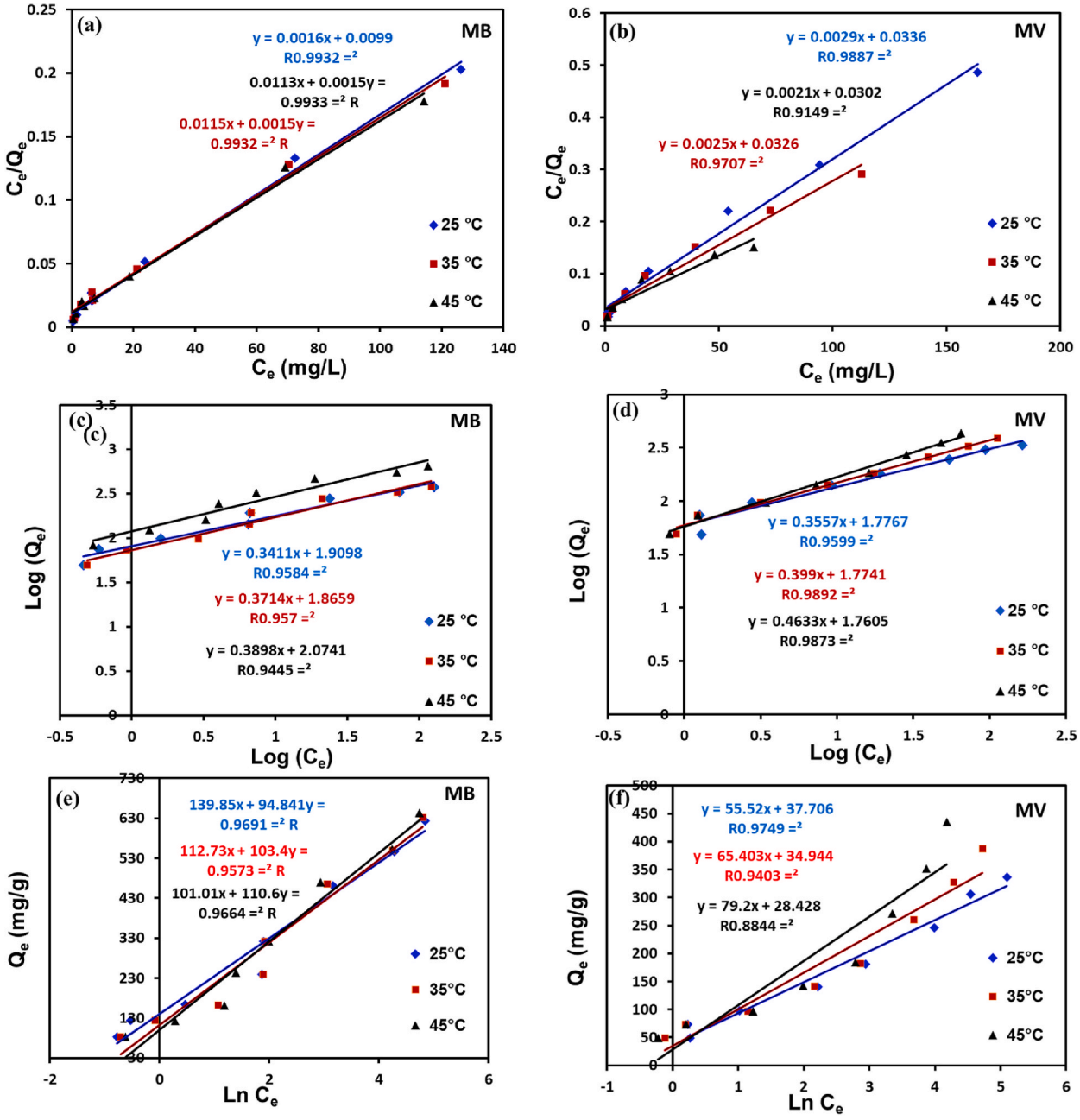

Fig. 6. Plots of Langmuir isotherm for the adsorption of MB (a) and MV (b), plots of Freundlich isotherm for the adsorption of MB (c) and MV (d), and plots of Temkin isotherm for the adsorption of MB (e) and MV (f) onto the ZSCS adsorbent.

the adsorption of MB and MV by kaolin/$CuFe_2O_4$ nanocompos [53] and bran sawdust/Fe_3O_4 composite [19].

3.2.2. *Effect of adsorbent dosage*

The effect of the amount of ZSCS on the adsorption of both MB and MV dyes was studied by varying the adsorbent dosage from 1 to 6 g/L under the parameter conditions (C_o = 50 mg/L, time = 1440 min, pH = 6; and T = 25 °C), as mentioned in Fig. 5a. The results showed that the removal efficiency of MB and MV dyes improved from (98.02 % and 91.12 %) to (99.26 % and 97.48 %) with the increase of the ZSCS adsorbent from 0.4 to 0.6 g/L and from 0.4 to 1 g/L, respectively, and then became constant with an increase in the amount of ZSCS to 6 g/L. The increase in adsorption capacity with growing adsorbent dose is due to the active availability of many sites on the surface of the ZSCS adsorbent [54,55]. However, this result revealed that an increase in the amount of ZSCS reduces the quantity of MB and MV adsorbed on ZSCS due to the adsorption capacity (mg/g) being inversely proportional to the amount of ZSCS in

Table 1
Isotherm parameters for the adsorption of MB and MV on ZSCS adsorbent.

Adsorbent	T (K)	$q_{e,exp.}$ (mg/g)	*Langmuir*			*Freundlich*			*Temkin*			
			q_m, (mg/g)	K_L (L/mg)	R^2	K_f, (mg/g) (L/mg)$^{1/n}$	n	R^2	A_T, L/mg	b_T (J/mole)	B	R^2
MB	298	628.83	625	0.162	0.9932	17.619	3.968	0.955	4.36	26.12	94.8	0.9691
	308	631.5	666.66	0.130	0.9932	19.985	4.545	0.982	2.50	23.45	112.7	0.9573
	318	643	666.66	0.132	0.9933	27.771	8.474	0.934	2.98	27.82	101.0	0.9664
MV	298	336.3	344.82	0.086	0.9887	9.106	4.739	0.954	1.97	44.62	55.5	0.9403
	308	387.36	400	0.076	0.9707	9.487	4.566	0.964	6.49	75.65	34.9	0.8924
	318	434.75	476.19	0.069	0.9149	10.485	4.291	0.888	1.43	35.48	79.2	0.8844

the calculated adsorption capacity equation (Eq. (2)) [56,57]. Similar results have been reported on the influence of adsorbent dosage on the adsorption of methylene blue by Paspalum maritimum (PMT) [58]. Therefore, 0.6 g/L for MB dye and 1 g/L for MV dye were selected as the optimal adsorbent dosage for future experiments.

3.2.3. Effect of contact time

The influence of contact time on the percentage removal of MB and MV dyes onto ZSCS adsorbent was examined at different interval times (5–120 min) under the parameter conditions (C_o = 50 mg/L, T = 25 °C, adsorbent dose = 0.6 g/L for MB and 1 g/L for MV, and pH = 6), as shown in Fig. 5b it was observed that 98.62 % and 97.46 % MB and MV can be removed within 5 min, suggesting the ultra-fast adsorption process of both MB and MV dyes from the aqueous solutions. Then, the removal efficiency of MB and MV dyes was increased slightly from 98.62 % to 99.16 % for MB dye and from 97.46 % to 97.74 % for MV dye when contact time increased from 5 to 30 min. The further increase of equilibrium time to 120 cannot enhance the MB and MV dye adsorption. This is due to the accumulation of MB and MV dye on the surface of the adsorbent, as well as the saturation of the adsorption sites [59]. Therefore, these findings suggest that the ZSCS adsorbent can adsorb MB and MV dye. Similar results have been reported on the influence of contact time on the adsorption of methylene blue by Paspalum maritimum (PMT) and *Cyanthilium cinereum* (L.) H. Rob [58]. Thus, 30 min was selected as the optimal equilibrium time for future experiments.

3.2.4. Effect of initial dye concentration and temperature

The influence of initial MB and MV dye concentrations on the adsorption process of MB and MV dye was tested in concentrations ranging from 50 to 500 mg/L at three temperatures, 298, 308, and 318 K, and constant parameter conditions (time = 30 min, pH = 6, and adsorbent dose = 0.6 g/L for MB dye and 1 g/L for MV), as shown in Fig. 5c and d. Results showed that the MB and MV adsorbed on ZSCS adsorbent improved from 82.56 to 48.70 mg/g to 622.83 and 336.3 mg/g, with an increase in the initial concentration of MB and MV dye from 50 to 500 mg/L, respectively, at 298 K. The improvement of ZSCS adsorption capacity at higher dye concentrations is due to the increased driving force for mass transfer from the solution to the surface of the ZSCS adsorbent. Fig. 6a shows the influence of different temperatures (298–318 K) on MB and MV adsorption efficiencies. As the temperature increased from 298 to 318 K, the quantity of MB and MV adsorbed on adsorbent increased slightly from 622.83 to 643 mg/g for MB dye and from 336.3 to 434.75 mg/g for MV dye at 500 mg/L, respectively, suggests that the adsorption of MB and MV onto adsorbent is endothermic. The increase in adsorption capacity with increasing temperature is likely due to the activation of the adsorption site and the high mass transfer rate from the bulk solution to the ZSCS surface [60]. A similar conclusion has been reported by Tong et al. (2016) and Sadiku et al.(2022) for the adsorption of methyl violet dye onto α-Fe_2O_3@Porous hollow carbonaceous microspheres [61] and halloysite nano-clay [18], respectively.

3.3. Adsorption isotherm

Three linear isotherm models, namely Langmuir (Eq. (3)), Freundlich (Eq. (4)), and Temkin (Eq. (5)) were employed to evaluate the adsorption performance of the ZSCS towards MB and MV removal. The above models are expressed in the following equations:

$$\frac{C_e}{q_e} = \frac{C_e}{Q_m} + \frac{1}{bQ_m} \tag{3}$$

$$\ln q_e = \ln K_f + \frac{1}{n} \ln C_e \tag{4}$$

$$q_e = \mathrm{RT} / b_T \ln(A_T C_e) \tag{5}$$

where q_e and q_m are the amounts of MB and MV adsorbed at equilibrium and maximum per unit weight of adsorbent (mg/g), respectively, Ce (mg/L) is the MB and MV dye concentration at equilibrium; K_L and K_F are Langmuir and Freundlich adsorption equilibrium constant. A_T is the Temkin equilibrium constant (L/g) corresponding to the maximum binding energy, b_T (J/mol) is Temkin's constant (related to heat of adsorption). The linear isotherm model is represented in Fig. 6(a–f), and the isotherm data parameters with their coefficients of determination (R^2) are listed in Table 1. Based on the highest value of R^2 ($R^2 > 0.99$) for both MB

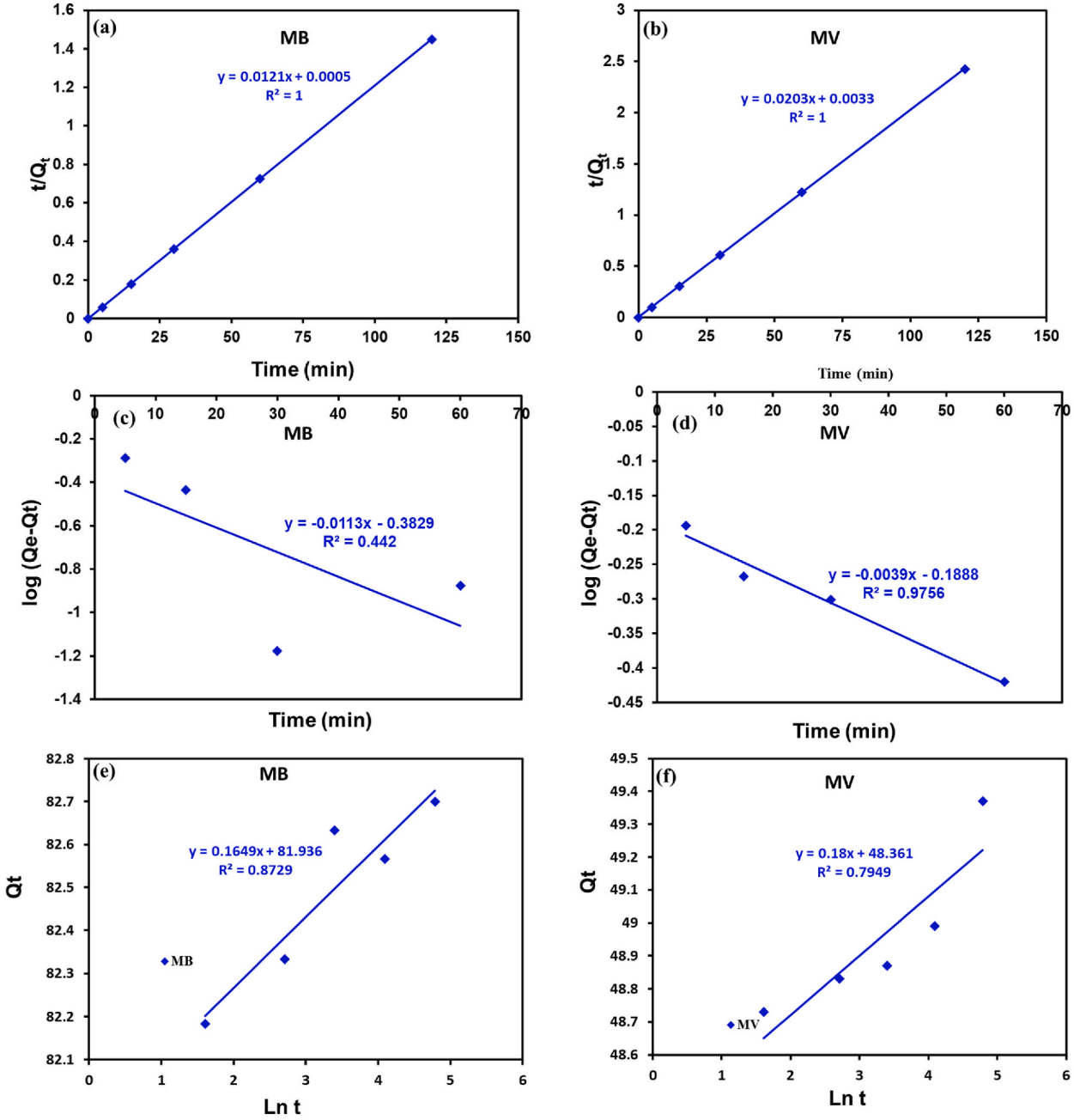

Fig. 7. Plot of pseudo-first-order for the adsorption of MB (a) and MV (b), plots of pseudo-second-order for the adsorption of MB (c) and MV (d), and plot of Elovich kinetics for the adsorption of MB (e) and MV (f) onto the ZSCS adsorbent.

and MV dyes, the Langmuir isotherm model was the best-fitting isotherm model for describing the adsorption of MB and MV dye on ZSCS, indicating that the adsorption process is monolayer adsorption with a maximum adsorption capacity of 666.66 for MB dye and 476.19 mg/g for MV dye. According to the Temkin isotherm model Fig. 6e and f, the values of b_T were greater than A_T values for both adsorptions of MB and MV indicating good interactions between dyes and ZSCS (Table 1). These results are in agreement with previous studies on the removal of methylene blue and methyl violet dyes using Hagenia abyssinica leaf powder (HALP) [62] and Raw date seeds [63], respectively.

3.4. Adsorption kinetics

To determine the proposed adsorption mechanism of MB and MV dye adsorption onto ZSCS, three kinetic models, namely, pseudo-

Table 2
Kinetic parameters for the adsorption of MB and MV on ZSCS adsorbent.

Dye	C_o (mg/L)	$q_{e,exp.}$ (mg/g)	Pseudo-first-order			Pseudo-second-order			Elovich		
			$q_{e1,\ cal.}$ (mg/g)	K_1 (1/min)	R^2	$q_{e2,\ cal.}$ (mg/g)	K_2 (g/mg-min)	R^2	α (mg/g min)	B (mg/g)	R^2
MB	50	82.56	0.414	0.026024	0.442	82.64	0.29282	1	39.62258181	0.012205	0.8279
MV	50	48.99	0.647	0.008982	0.9756	49.26	0.124876	1	24.05947373	0.020678	0.7949

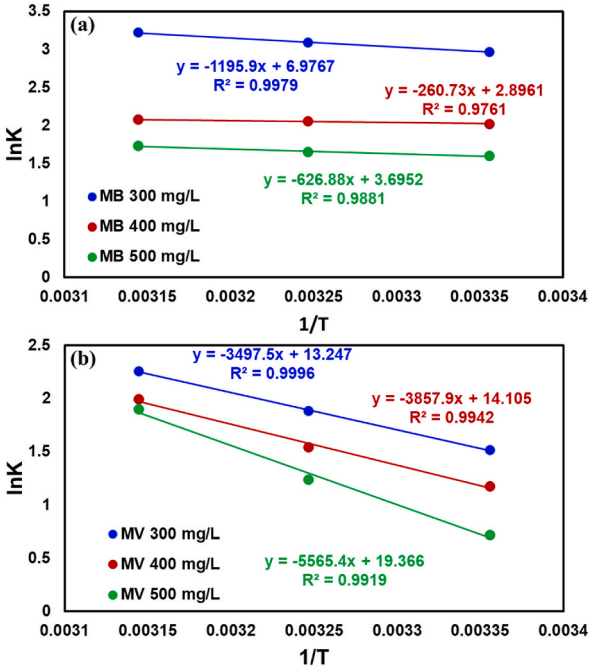

Fig. 8. Plot of ln Kc versus 1/T for the adsorption of MB (a) and MV (b) onto the ZSCS adsorbent.

first-order (PFO) (Eq. (6)), (pseudo-second-order (PSO), (Eq. (7)), and Elovich (Eq. (8)) were applied. The aforementioned models are expressed in the following equations:

$$\log(q_e - q_t) = \log q_e - \frac{k_1 t}{2.303} \tag{6}$$

$$\frac{t}{q_t} = \frac{1}{k_2 {q_e}^2} + \frac{t}{q_e} \tag{7}$$

$$q_t = 1/\beta \ln(1 + \alpha\beta t) \tag{8}$$

where, q_e and q_t (mg/g) are the amount of MB and MV adsorbed at equilibrium and time per unit weight of adsorbent, respectively, and k1 (1/min) and k2 (g/mg*min) are the adsorption rate constants of PFO and PSO models, respectively. α and β represent the initial adsorption rate and the desorption coefficient, respectively. The fitting kinetic model is represented in Fig. 7, and Table 2 shows the parameters of kinetic data with their coefficients of determination (R^2). Based on the highest value of the R^2, the pseudo-second-order model is the best-fitting kinetic model to describe the adsorption of MB and MV dye onto ZSCS. Additionally, the calculated adsorption capacity value by PSO (82.64 mg/g) is very close to the experimental value of adsorption capacity (82.56 mg/g), indicating chemisorption may be contributed to the adsorption of both MB and MV dyes on ZSCS. According to the Elovich model (Fig. 7e and f), the value of α was higher than β indicating a higher adsorption rate than desorption. A similar conclusion has been reported by Sadiku et al. (2022) and Tong et al. (2016) for the adsorption of MV dye onto halloysite nano-clay [18], and α-Fe_2O_3@Porous hollow carbonaceous microspheres [61], respectively.

3.5. Adsorption thermodynamics

The values of thermodynamic parameters, including standard free energy change (ΔG^o), standard enthalpy change (ΔH^o), and

Table 3
Thermodynamic parameters for the adsorption of MB and MV on ZSCS adsorbent.

Dye	Concentration MG dye	ΔH° (kJ/mol)	ΔS° (J/mol.K)	ΔG° (kJ/mol)		
				298 K	308 K	318 K
MB	300	9.94	58.00	−7.35	−7.90	−8.51
	400	2.17	24.07	−5.00	−5.26	−5.48
	500	5.21	30.72	−3.95	−4.22	−4.57
MV	300	29.07	110.13	−3.75	−4.82	−5.95
	400	32.07	117.26	−2.91	−3.95	−5.26
	500	46.27	161.00	−1.78	−3.16	−5.01

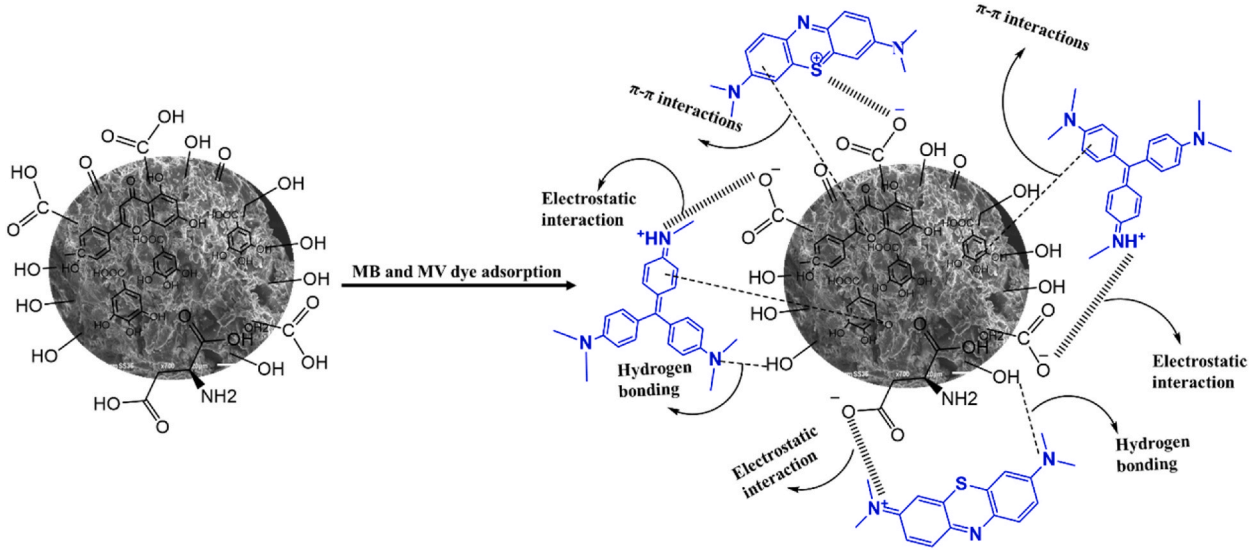

Fig. 9. Proposed adsorption mechanism of MB and MV dyes onto ZSCS adsorbent.

standard entropy change (ΔS^o), were calculated by the following equations (9) and (10):

$$\Delta G^\circ = -RT\,ln\,Kc \tag{9}$$

$$lnKc = -\frac{\Delta H^0}{RT} + \frac{\Delta S^0}{R} \tag{10}$$

where T is the absolute temperature (K), R (8.314 J mol^{-1} K^{-1}), and Kc is the thermodynamic equilibrium constant, equal qe/ce. The values of ΔH^o and ΔSo were calculated from the plot of ln Kc versus 1/T, as shown in Fig. 8a and b. The thermodynamic parameters are listed in Table 3. A positive value of ΔH^o change suggests that the adsorption of MB and MV dye by ZSCS is endothermic. Additionally, the ΔHo values ranged from 2.17 to 9.94 kJ/mol and from 29.07 to 46.27 kJ/mol, which are in the ΔH^o range for physisorption and chemisorption, respectively. A negative value of ΔG^o change indicates that the adsorption of MB and MV dye by ZSCS is thermodynamically feasible and spontaneous. A positive value of ΔS^o change reflects the increase of randomness in the adsorption system during the MB and MV adsorption onto ZSCS. A similar conclusion has been reported by Belete Geremew and Dagme Zewde (2022) [62].

3.6. Adsorption mechanism

The adsorption mechanism of MB and MV dyes on ZSCS surfaces depends on the nature of the surface charge of both adsorbent and absorbate. It can determine the interaction occurring between dyes (MB and MV) and ZSCS surface through the FTIR analysis of the ZSCS surface before and after the adsorption of MB and MV dyes. In addition, the effect of different parameters such as point zero charge of ZSCS and solution pH on the adsorption process were taken into consideration to explain the MB and MV adsorption mechanism, as shown in section 3.2.1. According to the FTIR analysis, the bands of functional groups such as – OH/-NH, -COO-, and C=C decreased in intensities from (3307, 1729, and 1615- 1511 cm^{-1}) to ((3312, 1725, and 1605-1511 cm^{-1}) and (3307, 1726, 1605-1511 cm^{-1}) after adsorption of MB and MV, respectively, confirmed that these surface functional groups are responsible for the adsorption of both dye molecules via π–π interactions, electrostatic interaction, and hydrogen bonding, as shown in Fig. 9.

Table 4
Comparison of maximum adsorption capacity of ZSCS adsorbent toward adsorption of MB and MV dyes with different adsorbents.

Adsorbent	MB, q_{max} (mg/g)	MV, q_{max} (mg/g)	Reference
MGO@TETA@MACS	247.37	–	[8]
CHt@MgO	252	–	[9]
Fe_3O_4@GO@AHSA	286.4	–	[16]
Modified rice husk (MRH)	–	154.49	[26]
Hagenia abyssinica leaf powder (HALP)	68.96		[62]
Porous carbon cross-linked zeolite nanocrystals	–	108.7	[64]
DTTS-POP	–	229.2	[65]
Multi-carboxylic magnetic gel (MMG)	458.7	400.0	[66]
Date seeds	–	59.5	[67]
Ziziphus spina-christi seed (ZSCS)	666.66	476.19	This study

3.7. Comparison with other adsorbents

The comparison of the obtained results in the present study with some recent studies for the removal of MB and MV dyes is shown in Table 4 [8,9,16,26,62–66]. It can be observed that the ZSCS displays a high adsorption capacity of 666.66 for MB and 476.19 mg/g for MV dye at 318 K compared to other adsorbents. The high adsorption capacity of the MB and MV in comparison with other adsorbents is attributed to the presence of the rich oxygenated compound and aromatic rings over the ZSCS surface, revealing that ZSCS can be considered a viable adsorbent for the removal of MB and MV dyes from aqueous solutions.

4. Conclusion

In this investigation, a cost-effective and readily available bio-absorbent was developed using ZSCS to eliminate MB and MV from aqueous solutions. The adsorption efficiency of ZSCS is significantly higher for MB removal compared to MV. The pH substantially affects the adsorption rate with the optimal pH 6. The maximum adsorption capacity of ZSCS for MB and MV dyes is 666.66 and 476.19 mg/g at 318 K, respectively. The amount of ZSCS adsorbent also influences the adsorption of MB and MV dyes, with 0.6 g/L for MB dye and 1 g/L for MV dye as the optimal dosage. It was found that 98.62 % and 97.46 % of MB and MV were removed within 5 min. The Langmuir isotherm model was the most suitable model for describing the adsorption of MB and MV dyes on ZSCS. Meanwhile, the pseudo-second-order model kinetic fits better to MB and MV adsorption onto ZSCS than other models, suggesting that the adsorption mechanism followed chemisorption.

Data availability statement

Data will be made available on request.

CRediT authorship contribution statement

Mohammed Alsuhybani: Visualization, Supervision, Methodology. **Musaad Aleid:** Resources, Project administration, Methodology, Data curation. **Reema Alzidan:** Methodology. **Khaled Bin Bander:** Resources, Funding acquisition. **Ayman Alrehaili:** Writing – review & editing, Writing – original draft, Supervision.

Declaration of competing interest

The authors declare that they have no known competing financial interests or personal relationships that could have appeared to influence the work reported in this paper.

Acknowledgment

The authors would like to express their gratitude to King Abdulaziz City for Science and Technology for providing the necessary laboratory resources and equipment for this study.

References

[1] Inamuddin, Xanthan gum/titanium dioxide nanocomposite for photocatalytic degradation of methyl orange dye, Int. J. Biol. Macromol. 121 (2019) 1046–1053, https://doi.org/10.1016/j.ijbiomac.2018.10.064.
[2] N. El Messaoudi, M. El Khomri, A. El Mouden, A. Bouich, A. Jada, A. Lacherai, H.M.N. Iqbal, S.I. Mulla, V. Kumar, J.H.P. Américo-Pinheiro, Regeneration and reusability of non-conventional low-cost adsorbents to remove dyes from wastewaters in multiple consecutive adsorption–desorption cycles: a review, Biomass Convers Biorefinery (2022), https://doi.org/10.1007/s13399-022-03604-9.
[3] S.S. Shah, B. Ramos, A.C.S.C. Teixeira, Adsorptive removal of methylene blue dye using biodegradable superabsorbent hydrogel polymer composite incorporated with activated charcoal, Water 14 (2022).

[4] M. Naushad, G. Sharma, Z.A. Alothman, Photodegradation of toxic dye using Gum Arabic-crosslinked-poly(acrylamide)/Ni(OH)2/FeOOH nanocomposites hydrogel, J. Clean. Prod. 241 (2019) 118263, https://doi.org/10.1016/j.jclepro.2019.118263.

[5] E.-R. Kenawy, A.A. Ghfar, S.M. Wabaidur, M.A. Khan, M.R. Siddiqui, Z.A. Alothman, A.A. Alqadami, M. Hamid, Cetyltrimethylammonium bromide intercalated and branched polyhydroxystyrene functionalized montmorillonite clay to sequester cationic dyes, J Environ Manage 219 (2018), https://doi.org/10.1016/j.jenvman.2018.04.121.

[6] F. Mojahedimotlagh, E.A. Nasab, R. Foroutan, D. Ranjbar Vakilabadi, S. Dobaradaran, E. Azamateslamtalab, B. Ramavandi, Azithromycin decomposition from simple and complex waters by H2O2 activation over a recyclable catalyst of clay modified with nanofiltration process brine, Environ. Technol. Innov. 33 (2024) 103512, https://doi.org/10.1016/j.eti.2023.103512.

[7] M. Naushad, A.A. Alqadami, Z.A. AlOthman, I.H. Alsohaimi, M.S. Algamdi, A.M. Aldawsari, Adsorption kinetics, isotherm and reusability studies for the removal of cationic dye from aqueous medium using arginine modified activated carbon, J. Mol. Liq. 293 (2019) 111442, https://doi.org/10.1016/j.molliq.2019.111442.

[8] I.H. Alsohaimi, M.S. Alhumaimess, A.A. Alqadami, H.M.A. Hassan, Q. Chen, M.S. Alamri, M.M.J. Alanzi, T.S. Alraddadi, Chitosan-carboxylic acid grafted multifunctional magnetic nanocomposite as a novel adsorbent for effective removal of methylene blue dye from aqueous environment, Chem. Eng. Sci. 280 (2023) 119017, https://doi.org/10.1016/j.ces.2023.119017.

[9] H. Majdoubi, A.A. Alqadami, R.E. Billah, M. Otero, B.-H. Jeon, H. Hannache, Y. Tamraoui, M.A. Khan, Chitin-Based magnesium oxide biocomposite for the removal of methyl orange from water, Int J Environ Res Public Health 20 (2023), https://doi.org/10.3390/ijerph20010831.

[10] A.A. Alqadami, M. Naushad, Z.A. Alothman, T. Ahamad, Adsorptive performance of MOF nanocomposite for methylene blue and malachite green dyes: kinetics, isotherm and mechanism, J Environ Manage 223 (2018) 29–36, https://doi.org/10.1016/j.jenvman.2018.05.090.

[11] H. Khatooni, S.J. Peighambardoust, R. Foroutan, R. Mohammadi, B. Ramavandi, Adsorption of methylene blue using sodium carboxymethyl cellulose-g-poly (acrylamide-co-methacrylic acid)/Cloisite 30B nanocomposite hydrogel, J. Polym. Environ. 31 (2023) 297–311, https://doi.org/10.1007/s10924-022-02623-x.

[12] R. Foroutan, S.J. Peighambardoust, D.C. Boffito, B. Ramavandi, Sono-photocatalytic activity of cloisite 30B/ZnO/Ag2O nanocomposite for the simultaneous degradation of crystal violet and methylene blue dyes in aqueous media, Nanomaterials 12 (2022), https://doi.org/10.3390/nano12183103.

[13] M.A. Khan, S.M. Wabaidur, M.R. Siddiqui, A.A. Alqadami, A.H. Khan, Silico-manganese fumes waste encapsulated cryogenic alginate beads for aqueous environment de-colorization, J. Clean. Prod. 244 (2020), https://doi.org/10.1016/j.jclepro.2019.118867.

[14] D.Ş. Arslan, H. Ertap, Z.M. Şenol, N. El Messaoudi, V. Mehmeti, Preparation of polyacrylamide titanium dioxide hybrid nanocomposite by direct polymerization and its applicability in removing crystal violet from aqueous solution, J. Polym. Environ. 32 (2024) 573–587, https://doi.org/10.1007/s10924-023-03004-8.

[15] S.J. Peighambardoust, D.C. Boffito, R. Foroutan, B. Ramavandi, Sono-photocatalytic activity of sea sediment@400/ZnO catalyst to remove cationic dyes from wastewater, J. Mol. Liq. 367 (2022) 120478, https://doi.org/10.1016/j.molliq.2022.120478.

[16] I. Hotan Alsohaimi, M.S. Alhumaimess, A. Abdullah Alqadami, G. Tharwi Alshammari, R. Fawzy Al-Olaimi, A.A. Abdeltawab, M.Y. El-Sayed, H.M. Hassan, Adsorptive performance of aminonaphthalenesulfonic acid modified magnetic-graphene oxide for methylene blue dye: mechanism, isotherm and thermodynamic studies, Inorg. Chem. Commun. 147 (2023) 110261, https://doi.org/10.1016/j.inoche.2022.110261.

[17] J. Mohanraj, D. Durgalakshmi, S. Balakumar, P. Aruna, S. Ganesan, S. Rajendran, M. Naushad, Low cost and quick time absorption of organic dye pollutants under ambient condition using partially exfoliated graphite, J. Water Process Eng. 34 (2020) 101078, https://doi.org/10.1016/j.jwpe.2019.101078.

[18] M. Sadiku, T. Selimi, A. Berisha, A. Maloku, V. Mehmeti, V. Thaçi, N. Hasani, Removal of methyl violet from aqueous solution by adsorption onto halloysite nanoclay: experiment and theory, Toxics 10 (2022), https://doi.org/10.3390/toxics10080445.

[19] H. Pooladi, R. Foroutan, H. Esmaeili, Synthesis of wheat bran sawdust/Fe3O4 composite for the removal of methylene blue and methyl violet, Environ. Monit. Assess. 193 (2021) 276, https://doi.org/10.1007/s10661-021-09051-9.

[20] T.S. Alomar, N. AlMasoud, G. Sharma, Z.A. Alothman, M. Naushad, Incorporation of trimetallic nanoparticles to the SiO2 matrix for the removal of methylene blue dye from aqueous medium, J. Mol. Liq. 336 (2021) 116274, https://doi.org/10.1016/j.molliq.2021.116274.

[21] Z. Ciğeroğlu, N. El Messaoudi, Z.M. Şenol, G. Başkan, J. Georgin, S. Gubernat, Clay-based nanomaterials and their adsorptive removal efficiency for dyes and antibiotics: a review, Mater Today Sustain 26 (2024) 100735, https://doi.org/10.1016/j.mtsust.2024.100735.

[22] P.O. Oladoye, T.O. Ajiboye, E.O. Omotola, O.J. Oyewola, Methylene blue dye: toxicity and potential elimination technology from wastewater, Results Eng 16 (2022) 100678, https://doi.org/10.1016/j.rineng.2022.100678.

[23] T. Tatarchuk, N. Danyliuk, A. Shyichuk, W. Macyk, M. Naushad, Photocatalytic degradation of dyes using rutile TiO2 synthesized by reverse micelle and low temperature methods: real-time monitoring of the degradation kinetics, J. Mol. Liq. 342 (2021) 117407, https://doi.org/10.1016/j.molliq.2021.117407.

[24] H. Mittal, A. Al Alili, S.M. Alhassan, M. Naushad, Advances in the role of natural gums-based hydrogels in water purification, desalination and atmospheric-water harvesting, Int. J. Biol. Macromol. 222 (2022) 2888–2921, https://doi.org/10.1016/j.ijbiomac.2022.10.067.

[25] T. Ahamad, M. Naushad, G.E. Eldesoky, S.I. Al-Saeedi, A. Nafady, N.S. Al-Kadhi, A.H. Al-Muhtaseb, A.A. Khan, A. Khan, Effective and fast adsorptive removal of toxic cationic dye (MB) from aqueous medium using amino-functionalized magnetic multiwall carbon nanotubes, J. Mol. Liq. 282 (2019) 154–161, https://doi.org/10.1016/j.molliq.2019.02.128.

[26] X. You, R. Zhou, Y. Zhu, D. Bu, D. Cheng, Adsorption of dyes methyl violet and malachite green from aqueous solution on multi-step modified rice husk powder in single and binary systems : characterization , adsorption behavior and physical interpretations, J. Hazard Mater. 430 (2022) 128445, https://doi.org/10.1016/j.jhazmat.2022.128445.

[27] S. Ravikumar, D. Mani, M. Rizwan Khan, N. Ahmad, P. Gajalakshmi, C. Surya, S. Durairaj, V. Pandiyan, Y.-H. Ahn, Effect of silver incorporation on the photocatalytic degradation of Reactive Red 120 using ZnS nanoparticles under UV and solar light irradiation, Environ. Res. 209 (2022) 112819, https://doi.org/10.1016/j.envres.2022.112819.

[28] M. Foroughi, S.J. Peighambardoust, B. Ramavandi, D.C. Boffito, Simultaneous anionic dyes degradation via H2O2 activation using Zeolite 4A/ZnO/Fe2(MoO4)3 nanoparticles in a sono-photocatalytic process, Adv. Powder Technol. 35 (2024) 104320, https://doi.org/10.1016/j.apt.2023.104320.

[29] M. Foroughi, S.J. Peighambardoust, B. Ramavandi, R. Foroutan, N.S. Peighambardoust, Simultaneous degradation of methyl orange and indigo carmine dyes from an aqueous solution using nanostructured WO3 and CuO supported on Zeolite 4A, Sep. Purif. Technol. 344 (2024) 127265, https://doi.org/10.1016/j.seppur.2024.127265.

[30] N. El Messaoudi, Z. Ciğeroğlu, Z.M. Şenol, A. Bouich, E.S. Kazan-Kaya, L. Noureen, J.H.P. Américo-Pinheiro, Chapter Fourteen - green synthesis of nanoparticles for remediation organic pollutants in wastewater by adsorption, in: A. Kumar, M. Bilal, L.F.R.B.T.-A. in C.P. Ferreira Environmental Management and Protection (Eds.), Recent Adv Wastewater Manag Nano-Based Remediat, Elsevier, 2024, pp. 305–345, https://doi.org/10.1016/bs.apmp.2023.06.016.

[31] R. EL Kaim Billah, A. Zaghloul, H.A. Ahsaine, A. BaQais, I. Khadoudi, N. El Messaoudi, M. Agunaou, A. Soufiane, R. Jugade, Methyl orange adsorption studies on glutaraldehyde cross-linking chitosan/fluorapatite-based natural phosphate composite, Int. J. Environ. Anal. Chem. (n.d.) 1–17. https://doi.org/10.1080/03067319.2022.2130690.

[32] R. Mohammadi, A. Saboury, S. Javanbakht, R. Foroutan, A. Shaabani, Carboxymethylcellulose/polyacrylic acid/starch-modified Fe3O4 interpenetrating magnetic nanocomposite hydrogel beads as pH-sensitive carrier for oral anticancer drug delivery system, Eur. Polym. J. 153 (2021) 110500, https://doi.org/10.1016/j.eurpolymj.2021.110500.

[33] Y.A. Bustos-Terrones, J.J. Hermosillo-Nevárez, B. Ramírez-Pereda, M. Vaca, J.G. Rangel-Peraza, V. Bustos-Terrones, M.N. Rojas-Valencia, Removal of BB9 textile dye by biological, physical, chemical, and electrochemical treatments, J. Taiwan Inst. Chem. Eng. 121 (2021) 29–37, https://doi.org/10.1016/j.jtice.2021.03.041.

[34] A.K.D. Alsukaibi, Various approaches for the detoxification of toxic dyes in wastewater, Processes 10 (2022), https://doi.org/10.3390/pr10101968.

[35] D.K. Sarfo, A. Kaur, D.L. Marshall, A.P. O'Mullane, Electrochemical degradation and mineralisation of organic dyes in aqueous nitrate solutions, Chemosphere 316 (2023) 137821, https://doi.org/10.1016/j.chemosphere.2023.137821.

[36] R. Foroutan, F.S. Khoo, B. Ramavandi, S. Abbasi, Heavy metals removal from synthetic and shipyard wastewater using phoenix dactylifera activated carbon, Desalin Water Treat 82 (2017) 146–156, https://doi.org/10.5004/dwt.2017.20908.

[37] M.A. Khan, M. Otero, M. Kazi, A.A. Alqadami, S.M. Wabaidur, M.R. Siddiqui, Z.A. Alothman, S. Sumbul, Unary and binary adsorption studies of lead and malachite green onto a nanomagnetic copper ferrite/drumstick pod biomass composite, J. Hazard Mater. 365 (2019) 759–770, https://doi.org/10.1016/j.jhazmat.2018.11.072.
[38] M.A. Khan, A.A. Alqadami, S.M. Wabaidur, M.R. Siddiqui, B.-H. Jeon, S.A. Alshareef, Z.A. Alothman, A.E. Hamedelniel, Oil industry waste based non-magnetic and magnetic hydrochar to sequester potentially toxic post-transition metal ions from water, J. Hazard Mater. 400 (2020) 123247, https://doi.org/10.1016/j.jhazmat.2020.123247.
[39] R. Foroutan, R. Mohammadi, J. Razeghi, M. Ahmadi, B. Ramavandi, Amendment of Sargassum oligocystum bio-char with MnFe2O4 and lanthanum MOF obtained from PET waste for fluoride removal: a comparative study, Environ. Res. 251 (2024) 118641, https://doi.org/10.1016/j.envres.2024.118641.
[40] Z.A.A. Moonis Ali Khan, Ayoub Abdullah Alqadami, Masoom Raza Siddiqui, Synthesis of hydrochar from jackfruit, US10557098B1, https://patents.google.com/patent/US10557098B1/en, 2020.
[41] N. El Messaoudi, A. El Mouden, M. El Khomri, A. Bouich, Y. Fernine, Z. Ciğeroğlu, J.H.P. Américo-Pinheiro, N. Labjar, A. Jada, M. Sillanpää, A. Lacherai, Experimental study and theoretical statistical modeling of acid blue 25 remediation using activated carbon from Citrus sinensis leaf, Fluid Phase Equilib 563 (2023) 113585, https://doi.org/10.1016/j.fluid.2022.113585.
[42] R. Foroutan, S.J. Peighambardoust, S. Ghojavand, S. Farjadfard, B. Ramavandi, Cadmium elimination from wastewater using potato peel biochar modified by ZIF-8 and magnetic nanoparticle, Colloid Interface Sci Commun 55 (2023) 100723, https://doi.org/10.1016/j.colcom.2023.100723.
[43] Z.M. Şenol, N. El Messaoudi, Y. Fernine, Z.S. Keskin, Bioremoval of rhodamine B dye from aqueous solution by using agricultural solid waste (almond shell): experimental and DFT modeling studies, Biomass Convers Biorefinery (2023), https://doi.org/10.1007/s13399-023-03781-1.
[44] B.H. Hameed, A.A. Ahmad, Batch adsorption of methylene blue from aqueous solution by garlic peel, an agricultural waste biomass, J. Hazard Mater. 164 (2009) 870–875, https://doi.org/10.1016/j.jhazmat.2008.08.084.
[45] M.T. Yagub, T.K. Sen, H.M. Ang, Equilibrium, kinetics, and thermodynamics of methylene blue adsorption by pine tree leaves, water, air, {&amp, Soil Pollut. 223 (2012) 5267–5282, https://doi.org/10.1007/s11270-012-1277-3.
[46] M.K. Uddin, A. Nasar, Walnut shell powder as a low- cost adsorbent for methylene blue dye : isotherm , kinetics , thermodynamic , desorption and response surface methodology examinations, Sci. Rep. (2020) 1–13, https://doi.org/10.1038/s41598-020-64745-3.
[47] A. Omri, M. Benzina, Removal of manganese (II) ions from aqueous solutions by adsorption on activated carbon derived a new precursor : Ziziphus spina-christi seeds, Alexandria Eng J 51 (2012) 343–350, https://doi.org/10.1016/j.aej.2012.06.003.
[48] S.A. Yousif, S. Al-mosawi, Adsorptive separation of dissolved cadmium from aqueous solution using (Ziziphus Spina-Christi) leaves as an adsorbent, South African, J. Chem. Eng. 42 (2022) 12–22, https://doi.org/10.1016/j.sajce.2022.07.002.
[49] M.S. Bashanaini, M.H. Al-douh, H.S. Al-ameri, Removal of malachite green dye from aqueous solution by adsorption using modified and unmodified local agriculture waste, Sci. J. Anal. Chem. 7 (2019) 42–56, https://doi.org/10.11648/j.sjac.20190702.12.
[50] G. Chen, X. Li, F. Saleri, M. Guo, Analysis of flavonoids in rhamnus davurica and its antiproliferative activities, Molecules 21 (2016), https://doi.org/10.3390/molecules21101275.
[51] G. Nigussie, M. Alemu, F. Ibrahim, Y. Werede, M. Tegegn, S. Neway, M. Endale, Phytochemicals, traditional uses and pharmacological activity of rhamnus prinoides: a review, Int J Second Metab 8 (2021) 136–151, https://doi.org/10.21448/ijsm.833554.
[52] T. Wahyono, D.A. Astuti, I.K. Gede Wiryawan, I. Sugoro, A. Jayanegara, Fourier transform mid-infrared (FTIR) spectroscopy to identify tannin compounds in the panicle of sorghum mutant lines, IOP Conf. Ser. Mater. Sci. Eng. 546 (2019) 42045, https://doi.org/10.1088/1757-899X/546/4/042045.
[53] R. Foroutan, S.J. Peighambardoust, S. Ghojavand, M. Foroughi, A. Ahmadi, F. Bahador, B. Ramavandi, Development of a magnetic orange seed/Fe3O4 composite for the removal of methylene blue and crystal violet from aqueous media, Biomass Convers Biorefinery (2023), https://doi.org/10.1007/s13399-023-04692-x.
[54] M. Alizadeh, S.J. Peighambardoust, R. Foroutan, Efficacious adsorption of divalent nickel ions over sodium alginate-g-poly(acrylamide)/hydrolyzed Luffa cylindrica-CoFe2O4 bionanocomposite hydrogel, Int. J. Biol. Macromol. 254 (2024) 127750, https://doi.org/10.1016/j.ijbiomac.2023.127750.
[55] J. Georgin, D. Franco, F.C. Drumm, P. Grassi, M.S. Netto, D. Allasia, G.L. Dotto, Powdered biosorbent from the mandacaru cactus (cereus jamacaru) for discontinuous and continuous removal of Basic Fuchsin from aqueous solutions, Powder Technol. 364 (2020) 584–592, https://doi.org/10.1016/j.powtec.2020.01.064.
[56] J.S. Algethami, A.A. Alqadami, S. Melhi, M.A.M. Alhamami, A.M. Fallatah, M.A. Rizk, Sulfhydryl functionalized magnetic chitosan as an efficient adsorbent for high-performance removal of Cd(II) from water: adsorption isotherms, kinetic, and reusability studies, Adsorpt. Sci. Technol. 2022 (2022) 2248249, https://doi.org/10.1155/2022/2248249.
[57] J.S. Algethami, M.A.M. Alhamami, A.A. Alqadami, S. Melhi, A.F. Seliem, Adsorptive performance of a new magnetic hydrochar nanocomposite for highly efficient removal of cadmium ions from water: mechanism, modeling, and reusability studies, Environ. Technol. Innov. 32 (2023) 103404, https://doi.org/10.1016/j.eti.2023.103404.
[58] F. Silva, L. Nascimento, M. Brito, K. da Silva, W. Paschoal, R. Fujiyama, Biosorption of methylene blue dye using natural biosorbents made from weeds, Materials 12 (2019), https://doi.org/10.3390/ma12152486.
[59] M. Alizadeh, S.J. Peighambardoust, R. Foroutan, H. Azimi, B. Ramavandi, Surface magnetization of hydrolyzed Luffa Cylindrica biowaste with cobalt ferrite nanoparticles for facile Ni2+ removal from wastewater, Environ. Res. 212 (2022) 113242, https://doi.org/10.1016/j.envres.2022.113242.
[60] M.A. Khan, A.A. Alqadami, S.M. Wabaidur, B.-H. Jeon, Co-carbonized waste polythene/sugarcane bagasse nanocomposite for aqueous environmental remediation applications, Nanomaterials 13 (2023), https://doi.org/10.3390/nano13071193.
[61] Z. Tong, P. Zheng, B. Bai, H. Wang, Y. Suo, Adsorption performance of methyl violet via α-Fe2O3@Porous hollow carbonaceous microspheres and its effective regeneration through a fenton-like reaction, Catalysts 6 (2016), https://doi.org/10.3390/catal6040058.
[62] B. Geremew, D. Zewde, Hagenia abyssinica leaf powder as a novel low-cost adsorbent for removal of methyl violet from aqueous solution: optimization, isotherms, kinetics, and thermodynamic studies, Environ. Technol. Innov. 28 (2022) 102577, https://doi.org/10.1016/j.eti.2022.102577.
[63] N.S. Ali, N.M. Jabbar, S.M. Alardhi, H.S. Majdi, T.M. Albayati, Adsorption of methyl violet dye onto a prepared bio-adsorbent from date seeds: isotherm, kinetics, and thermodynamic studies, Heliyon 8 (2022) e10276, https://doi.org/10.1016/j.heliyon.2022.e10276.
[64] S.M. Al-Jubouri, H.A. Al-Jendeel, S.A. Rashid, S. Al-Batty, Green synthesis of porous carbon cross-linked Y zeolite nanocrystals material and its performance for adsorptive removal of a methyl violet dye from water, Microporous Mesoporous Mater. 356 (2023) 112587, https://doi.org/10.1016/j.micromeso.2023.112587.
[65] S. Alavinia, R. Ghorbani-Vaghei, S. Asadabadi, A. Atrian, Sodium alginate/diethyleneamine-triazine-sulfonamide nanocomposite for adsorptive removal of Pb (II) and methyl violet from aqueous solutions, Mater. Chem. Phys. 293 (2023) 126915, https://doi.org/10.1016/j.matchemphys.2022.126915.
[66] Y. Song, Y. Duan, L. Zhou, Multi-carboxylic magnetic gel from hyperbranched polyglycerol formed by thiol-ene photopolymerization for efficient and selective adsorption of methylene blue and methyl violet dyes, J. Colloid Interface Sci. 529 (2018) 139–149, https://doi.org/10.1016/j.jcis.2018.06.005.